When Mathematics Meets Astrophysics

Analyzing the Number of Solutions to the Gravitational Lens Equation

Aniruddha Madhava
Advisor: Professor Charles Keeton

Rutgers University, Department of Physics and Astronomy, 136 Frelinghuysen Rd., Piscataway, NJ 08854 USA

(Dated: April 4, 2025)

Abstract

Gravitational lensing is a General Relativistic effect where a foreground mass distribution (e.g., a galaxy) distorts and magnifies light from distant sources. Lensing can also produce multiple images of the same source. To understand the properties of a lensed source, we must accurately model the lens system, which requires us to account for all lensed images. This leads to the mathematical problem of bounding the number of images. We analyzed this problem in the Newtonian framework. We derived the deflection angle for a single mass and showed that it is finite, necessitating modifications to existing mathematical analyses. We developed a routine to compute the angle for multiple masses in a single plane. Using two-dimensional root finding and the Virbhadra-Ellis lens equation, which is a relationship between the source and image positions, we constructed configurations that saturate known bounds on the number of images, laying a foundation for subsequent mathematical analyses.

1 Introduction

Gravitational lensing is the General Relativistic phenomenon in which light rays "bend" around a mass distribution due to the spacetime curvature it imposes. Although this effect was first proposed and briefly studied by 18th and 19th-century physicists like Isaac Newton and Johann von Soldner, the first correct theory and predictions were not made until 1915 using Albert Einstein's new Theory of General Relativity. The first observation came four years later during Arthur Eddington's famed 1919 solar eclipse expedition. In the 106 years since, gravitational lensing has transformed from a cosmic peculiarity to a major astrophysical tool.

This transformation is partly due to gravitational lensing's ability to magnify and produce multiple images of distant sources, providing rare glimpses into an unobservable universe. For instance, in *strong gravitational lensing*, a galaxy cluster between the source and the observer produces complicated configurations of multiple images of distant sources. In *gravitational microlensing*, distant point-like sources are lensed by a collection of compact bodies like stars and black holes [10]. The granular distribution of these bodies can produce various numbers of images depending on the

source's angular position in the plane of the sky. Studying these images enables astrophysicists to understand physical conditions in the distant and early universe.

For example, [4] and the JWST PEARLS team reported an unanticipated diversity in the properties of galaxies strongly lensed by the El Gordo galaxy cluster (ACT-CL J0102-4915). Meanwhile, [9] reported the discovery of a terrestrial-mass rogue planet microlensed by a compact object roughly the size of the Earth. Likewise, microlensing of distant quasars produces observable variations in their brightnesses, which can help us understand their physical properties [10].

To interpret and reconstruct distant sources microlensed by compact bodies, it is necessary to understand and capture the lensing distortions and magnifications caused by these bodies through *lens models*. While a considerable amount of work has studied ways to improve lens models [8, 12, 13, 17], one important common factor in these works is a proper accounting of the total number of lensed images produced.

From a mathematical standpoint, analyzing variations of this problem under assumptions like the Newtonian theory of gravitation, the Born approximation, and the small-angle approximation for different classes of lens systems leads to many interesting results. For instance, [10] showed there are exactly two lensed images for a single point-mass using differential topology and Morse Theory. For a collection of $g > 1$ point masses on a single plane, [7, 10, 14] showed that the number of lensed images is at least $g+1$, and at most $5g-5$. However, in some sense, these results are incorrect in the complete General Relativistic (GR) framework. An analysis of gravitational lensing by a point mass in the Schwarzschild metric reveals that there are two "principal" images, and infinitely more "relativistic" images that correspond to light rays that loop around a black hole $n \in \mathbb{N}$ times[3]. This suggests a breakdown when going from the complete relativistic framework to the specific assumptions used in previous work that must be rigorously analyzed.

Therefore, we studied the full-angle Virbhadra-Ellis gravitational lens equation [16] in the Newtonian framework without the Born, Small-Angle, and Thin-Lens approximations. While a mathematically rigorous analysis of the equation was out of scope of this project, we provided a numerical framework for future mathematical analysis of this problem. We examined whether the existing mathematical framework developed in [10] can be used to determine a lower bound on the number of solutions by constructing the deflection angle for a single point mass. We also examined the possibility of multiple image formation and if the number of solutions to our equation satisfies the $g+1 \leq N \leq 5g-5$ inequality. While we conjecture that our equation satisfies the same bounds, we also show that we must modify existing mathematical proofs for the lower bound, which could lead to new and interesting connections within mathematics, and between mathematics and astrophysics. In Section 2, we discuss various components of our methodology. Section 3 discusses our results, and Section 4 discusses our conclusions and provides implications for future work

2 Methodology

2.1 A Mathematical Problem

We consider the physical configuration depicted in Figure 1. Let $g \geq 1$ be a positive integer, $\boldsymbol{\xi}_1, \ldots, \boldsymbol{\xi}_g$ be infinite singularities in a potential $\psi : L \to \mathbb{R}$, and $m_1, \ldots, m_g$ be their "masses". Define $\boldsymbol{\beta} : L \to S$ to be the map,

$$\boldsymbol{\beta}(\boldsymbol{\theta}) = \boldsymbol{\theta} - \sum_{j=1}^{g} m_j \frac{\boldsymbol{\theta} - \boldsymbol{\xi}_j}{\left|\boldsymbol{\theta} - \boldsymbol{\xi}_j\right|^2}. \tag{1}$$

This equation is the *small-angle* gravitational lens equation. For future reference, we denote

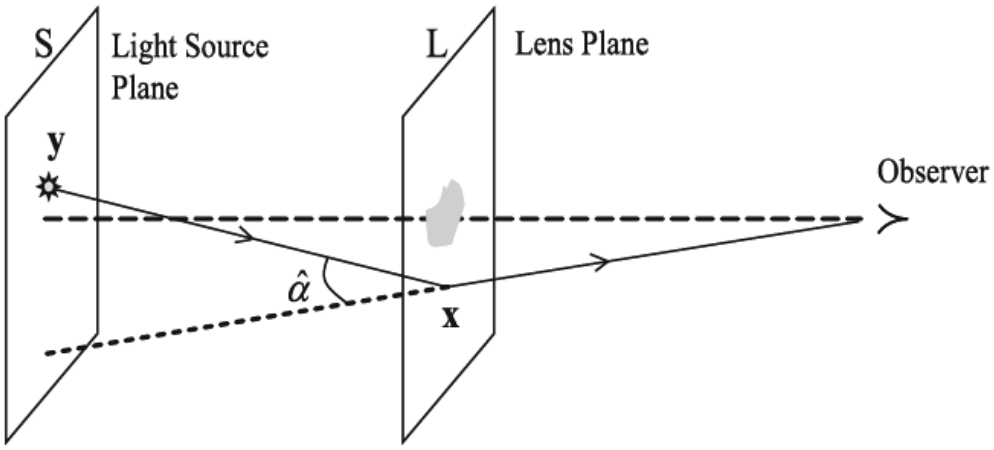

Figure 1: Depiction of gravitational lensing. For future reference, $\boldsymbol{\beta} \coloneqq \mathbf{y}$ and $\boldsymbol{\theta} \coloneqq \mathbf{x}$. This figure is borrowed from [11].

the second term on the right side of the equation by $(d_{LS}/d_S)\hat{\boldsymbol{\alpha}}$, where d_{LS} is the distance between L and S, d_L is the distance between the observer and L, and $d_S = d_{LS} + d_L$[1]. This term signifies the total deflection angle of a light ray coming from a distant source.

In this context, Eq. (1) is a relationship between the angular position of the source in the plane of the sky $\boldsymbol{\beta}$, the image positions $\boldsymbol{\theta}$, and the total deflection that an incoming light ray experiences $(d_{LS}/d_S)\hat{\boldsymbol{\alpha}}$. Physically, light rays from a distant source originate in S and pass through L before reaching the observer. However, since multiple images of a source are possible, a map from S to L is generally one-to-many, and is not a well-defined function. However, the inverse map $\boldsymbol{\beta} : L \to S$ maps each image $\boldsymbol{\theta}$ in L to a single point $\boldsymbol{\beta}$ in S, and is well-defined. Now, we make the following definitions [11]:

Definition 2.1 (Critical Points of $\boldsymbol{\beta}$)**.** We define the set of *critical points* of $\boldsymbol{\beta}$, denoted $\text{crit}(\boldsymbol{\beta})$ to be the set

$$\text{crit}(\boldsymbol{\beta}) \coloneqq \{\boldsymbol{\theta} \in L : \det[\text{Jac}\, \boldsymbol{\beta}](\boldsymbol{\theta}) = 0\}\,. \tag{2}$$

Astrophysically, the set of critical points of $\boldsymbol{\beta}$ consists of all the points in the lens plane L that are infinitely magnified by gravitational lensing.

Definition 2.2 (Caustic points of $\boldsymbol{\beta}$)**.** We define the set of *caustic points* of $\boldsymbol{\beta}$ as the image of $\text{crit}(\boldsymbol{\beta})$ under $\boldsymbol{\beta}$:

$$\text{caus}(\boldsymbol{\beta}) \coloneqq \boldsymbol{\beta}\,(\text{crit}(\boldsymbol{\beta})) \subset S.$$

Astrophysically, these are the set of all possible source positions that can produce an infinitely magnified image.

Then [10], [7, 14] obtained the following results, respectively:

Theorem 1 (Lower Bound on the Number of Solutions)**.** If $\mathbf{y} = \boldsymbol{\beta}(\boldsymbol{\theta})$ is not in a caustic of $\boldsymbol{\beta}$, and the set of critical points of $\boldsymbol{\beta}$ is bounded and consists of only folds and cusps (see Figure 2 for

[1]Formally, this "sum rule" does not apply to *angular diameter distances*, which are typically used in the lens equation. However, since our system consists of point masses, we can assume that the spacetime outside of these masses is sufficiently flat, in which case this rule holds.

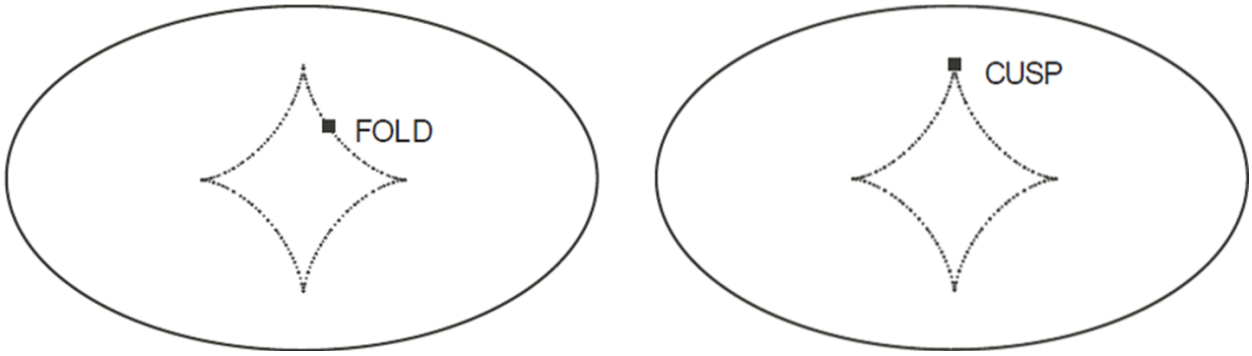

Figure 2: Caustic curves corresponding to critical curves containing folds (left) and cusps (right). This figure is adapted from [1].

examples), then for sufficiently large $\mathbf{y}$, the lower bound on the number of solutions to Eq. (1) is attained: $N = g + 1$.

Theorem 2 (Upper Bound on the Number of Solutions)**.** If $g \geq 2$ and $\mathbf{y} = \boldsymbol{\beta}(\boldsymbol{\theta})$ is not in a caustic of $\boldsymbol{\beta}$, then the number of solutions to Eq. (1) satisfies the upper bound, $N \leq 5g - 5$.

It has been shown that by Fermat's Principle, the solutions to Eq. (1) are precisely the critical points of the *time-delay map*, $T_{\boldsymbol{\beta}} : L \to \mathbb{R}$ [2, 15]. Physically, $T_{\boldsymbol{\beta}}$ provides a measure of the delay in the time taken by a light ray emitted by a distance source in S in reaching the observer because of the extra distance that it must travel due to a bend in its trajectory and the gravitational time dilation the light ray experiences as it passes through the gravitational wells of the masses.

For instance, the time-delay map corresponding to Eq. (1) is,

$$T_{\boldsymbol{\beta}}(\boldsymbol{\theta}) = \frac{1}{2}\left|\boldsymbol{\theta} - \boldsymbol{\beta}\right|^2 - \sum_{j=1}^{g} m_j \log\left|\boldsymbol{\theta} - \boldsymbol{\xi}_j\right|. \tag{3}$$

To find the critical points of $T_{\boldsymbol{\beta}}$, we look for the roots of its gradient.

$$\begin{aligned} &\nabla T_{\boldsymbol{\beta}} = \boldsymbol{\theta} - \boldsymbol{\beta} - \sum_{j=1}^{g} m_j \frac{\boldsymbol{\theta} - \boldsymbol{\xi}_j}{\left|\boldsymbol{\theta} - \boldsymbol{\xi}_j\right|^2} = \mathbf{0}. \\ \implies &\boldsymbol{\theta} - \boldsymbol{\beta} - \sum_{j=1}^{g} m_j \frac{\boldsymbol{\theta} - \boldsymbol{\xi}_j}{\left|\boldsymbol{\theta} - \boldsymbol{\xi}_j\right|^2} = \mathbf{0}. \\ \implies &\boldsymbol{\beta} = \boldsymbol{\theta} - \sum_{j=1}^{g} m_j \frac{\boldsymbol{\theta} - \boldsymbol{\xi}_j}{\left|\boldsymbol{\theta} - \boldsymbol{\xi}_j\right|^2}, \end{aligned} \tag{4}$$

where the last equation is Eq. (1).

Therefore, to find the total number of solutions to Eq. (1), it suffices to examine the number of critical points of $T_{\boldsymbol{\beta}}$. [10] reported that the number of such points are constrained by the *Betti numbers*, B_0, B_1, and B_2, which are *topological invariants* of a surface. Intuitively, the k^{th} Betti number, B_k, represents the number of k-dimensional holes in a surface[2]. While a complete discussion of the theory of Betti numbers requires differential topology and Morse Theory, calculating the Betti

[2]https://www.quantamagazine.org/topology-101-how-mathematicians-study-holes-20210126/

numbers provides a series of inequalities, called the *Morse inequalities*. [10] then showed that these inequalities readily imply the lower bound referenced in Theorem 1. However, the key requirement for these inequalities to hold is that the time-delay surface, and hence the deflection angle $\hat{\boldsymbol{\alpha}}$ *must* diverge at each of the point masses m_j. We can see this in Eq. (3) since $\lim_{\boldsymbol{\theta}\to\boldsymbol{\xi}_j} \log\left|\boldsymbol{\theta}-\boldsymbol{\xi}_j\right| \to -\infty$.

On the other hand, verifying the upper bound referenced in Theorem 2 requires elements of complex and harmonic analysis. While [14] provided explicit constructions of physical configurations that saturated the upper bound, [7] explicitly studied this bound for a more general family of harmonic rational functions and demonstrated that Eq. (1) belonged to this family.

2.2 Our Analysis

2.2.1 Background

Eq. (1), studied by [7, 10, 14], implicitly assumes three approximations: (1) the small-angle approximation, (2) the Born approximation, and (3) the Thin-Lens approximation. In the small-angle approximation, we assume that the angular positions of the sources and images, and the deflection angle $\hat{\boldsymbol{\alpha}}$ have sufficiently small magnitudes ($\ll 1$ rad). While this assumption is sufficient for general gravitational lensing configurations, some systems, particularly those involving large deflections of rays passing close to a compact body like a black hole, may not be modeled accurately by the approximation. Likewise, the Born approximation, in which we calculate the total deflection by computing the total impulse acting on a light ray along the **undeflected** trajectory, and the Thin-Lens approximation, in which we assume that a light ray bends only as it passes the lens, may not be the correct pictures of gravitational lensing for more general configurations.

Therefore, we studied the *full-angle* Virbhadra-Ellis lens equation [16]:

$$\tan(\boldsymbol{\beta}) = \tan(\boldsymbol{\theta}) - \frac{d_{LS}}{d_S}\left(\tan(\boldsymbol{\theta}) + \tan\left(\hat{\boldsymbol{\alpha}}-\boldsymbol{\theta}\right)\right). \tag{5}$$

Figure 3 depicts the lensing geometry with each of the angles (note that the figure depicts the Thin-Lens approximation, although neither Eq. (5) nor our analysis uses this approximation), and compares our work with previous research.

Assuming the small-angle approximation (i.e., $\boldsymbol{\beta}, \boldsymbol{\theta}, \hat{\boldsymbol{\alpha}} \ll 1$ rad, and $\tan(x) \approx x$) enables us to recover Eq. (1).

Unlike [7, 10, 14], we work in the Newtonian framework of gravity, whereby we assume Newton's law of universal gravitation, and a corpuscular picture of the photon with mass $\tilde{m} \to 0$. While the Newtonian framework is not the correct picture of gravity and gravitational lensing and is therefore not immediately applicable to astrophysics, Eq. (5) is still interesting mathematically and provides a numerical framework upon which similar work in the full relativistic framework can be done in the future.

To find the deflection angle $\hat{\boldsymbol{\alpha}}$ due to a system of g point-masses $m_1, \ldots, m_g$ in L, we first calculate the trajectory of a photon coming from infinity in the $+\hat{x}$-direction by solving the following differential equation:

$$\begin{cases} \dfrac{d^2\mathbf{r}}{dt^2} = -G\displaystyle\sum_{j=1}^{g} M_j \frac{\mathbf{r}-\boldsymbol{\xi}_j}{\left|\mathbf{r}-\boldsymbol{\xi}_j\right|^3}, \\ \mathbf{r}(0) = (-\infty, b_y, b_y), \\ \dot{\mathbf{r}}(0) = (c, 0, 0), \end{cases} \tag{6}$$

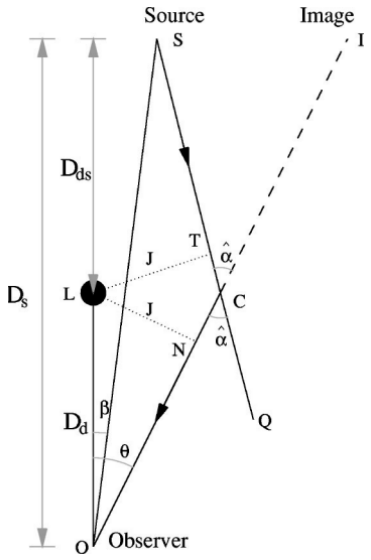

	Previous Work	Our Work
Newtonian	×	✓
Small-Angle	✓	×
Born	✓	×
Thin-Lens	✓	×

Figure 3: (Left) Schematic depiction of gravitational lensing. The sharp bend at C depicts the Thin-Lens approximation. **(Right)** A comparison of our work with previous research.

where $\mathbf{b} = (b_y, b_z)$ is the impact parameter and c is the speed of light. Then we calculate the difference between the initial and final slopes to find the deflection angle. We note that the deflection angle $\hat{\boldsymbol{\alpha}}$ is a two-dimensional vector in L. The components of $\hat{\boldsymbol{\alpha}}$ are given in Eq. (7).

$$\hat{\alpha}_i = \arctan\left(\frac{r_i(t_f) - r_i(t_f - \delta t)}{r_x(t_f) - r_x(t_f - \delta t)}\right) - \arctan\left(\frac{r_i(\delta t) - r_i(0)}{r_x(\delta t) - r_x(0)}\right), \qquad i = y, z. \tag{7}$$

We solve the differential equation, Eq. (6) over the time interval $[0, t_f]$, for sufficiently large t_f.

2.2.2 Overview of Questions

Through our analysis, we sought to answer the following questions:

- **Q_I** : Can the original proof of the lower bound by [10] be readily adapted to our equation? That is, does our deflection angle diverge near each point mass?
- **Q_{II}** : Can our gravitational lens equation produce infinitely many "relativistic" images as in the complete General Relativistic framework?
- **Q_{III}** : Can our lens equation have multiple solutions? If so, how do these images compare with image positions predicted by the relativistic framework adopted by [7, 10, 14]?
- **Q_{IV}** : If we can produce multiple images, can we also produce lens configurations that saturate the existing lower and upper bounds?

To answer these questions, we used the following steps:

1. Derive a closed-form expression for the Newtonian deflection angle for a single point mass.
2. Develop a numerical routine (`deflecThor`) to calculate the deflection angles for g point-masses using Eq. (6).
3. Use `deflecThor`, `pygravlens` (routine that finds images for the small-angle GR lens equation[3]), and 2D root finding to find solutions to Eq. (5).

[3]https://github.com/chuckkeeton/pygravlens/blob/main/pygravlens.py

We discuss each of these steps in the following subsections.

2.2.3 The Newtonian Deflection Angle

Assuming energy and angular momentum conservation, we find that the deflection angle of a light ray due to a single point mass M at the origin is given by the equation (see Appendix A for details on the derivation),

$$|\hat{\boldsymbol{\alpha}}(b)| = 2\arcsin\left(\frac{\tilde{r}}{\sqrt{\tilde{r}^2 + b^2}}\right), \tag{8}$$

where $\tilde{r} = (1/2)r_s = GM/c^2$ is half the Schwarzschild radius r_s, and b is the impact parameter. We note that von Soldner predicted that a light ray grazing the surface of the sun ($b = R_\odot$) would have a deflection angle half the value predicted by Einstein's Theory of General Relativity, which was $4GM/c^2b$ (to first-order). To check if Eq. (8) is consistent with this prediction, we Taylor expand the expression around $\tilde{r} = 0$. Doing so, we find

$$|\hat{\boldsymbol{\alpha}}(b)| = \frac{2\tilde{r}}{b} - \frac{2\tilde{r}^3}{3b^3} + \mathcal{O}(\tilde{r}^5) \implies |\hat{\boldsymbol{\alpha}}(b)| \approx \frac{2\tilde{r}}{b} = \frac{2GM}{c^2 b}. \tag{9}$$

2.2.4 The `deflecThor` Routine

The deflection angle in Eq. (8) holds only for a single point mass lens at the origin. To obtain the angle for a general configuration consisting of g lenses, we need to solve the differential equation, Eq. (6) numerically. Therefore, we wrote the routine, `deflecThor()`, which calculates the trajectory of a light ray given the initial position of the source in the plane of the sky (y_0, z_0), the masses of the lenses, and their positions in the plane of the sky $(y_{l,0}, z_{l,0})$ in physical (i.e., SI) units. `deflecThor` assumes that all of the lenses are fixed at $x = 0$, while the source is situated at some $x_0 < 0$.

As illustrated in the integral formulation of the Newtonian deflection angle (Eq. 19) and the second initial condition in Eq. (6), we require the light ray to travel inwards from $-\infty$ towards the sources at $x = 0$. Numerically, we cannot integrate from $x_0 = -\infty$ using `scipy.integrate.solve_ivp`; however, it suffices to pick a sufficiently negative x_0.

To pick x_0, we ran multiple lensing simulations of a light ray passing close to a single mass at the origin for various impact parameters, b. Then we compared our results for the deflection angle with the angles predicted by the General Relativistic deflection angle, noting that the Newtonian angles should be half the relativistic values. We found that for configurations with $b \leq 100$ km, the ideal x_0 for accuracy and efficiency was $-10^{5.81}$ meters, while for $b > 100$ km, the ideal x_0 was -7×10^{10} meters. Therefore, we added an algorithm in `deflecThor` to calculate the total distance between the source and each of the lenses in the plane, find the minimum distance, and set x_0 accordingly.

Next, while we did not explicitly build energy and angular momentum conservation into our routine, we were interested in seeing if these conditions were satisfied since the derivation of the single mass deflection angle, Eq. (8), requires both (see Section A). To do so, we calculated the trajectory of a light ray for various configurations, and computed the total energy and angular momentum (see Eq. 14) at constant time steps. Figure 4 shows the results for the configuration used to produce the last plot in Figure 9. We found that while the total energy and angular momentum vary, the fractional changes are very small and attributable to numerical errors associated with numerical integration.

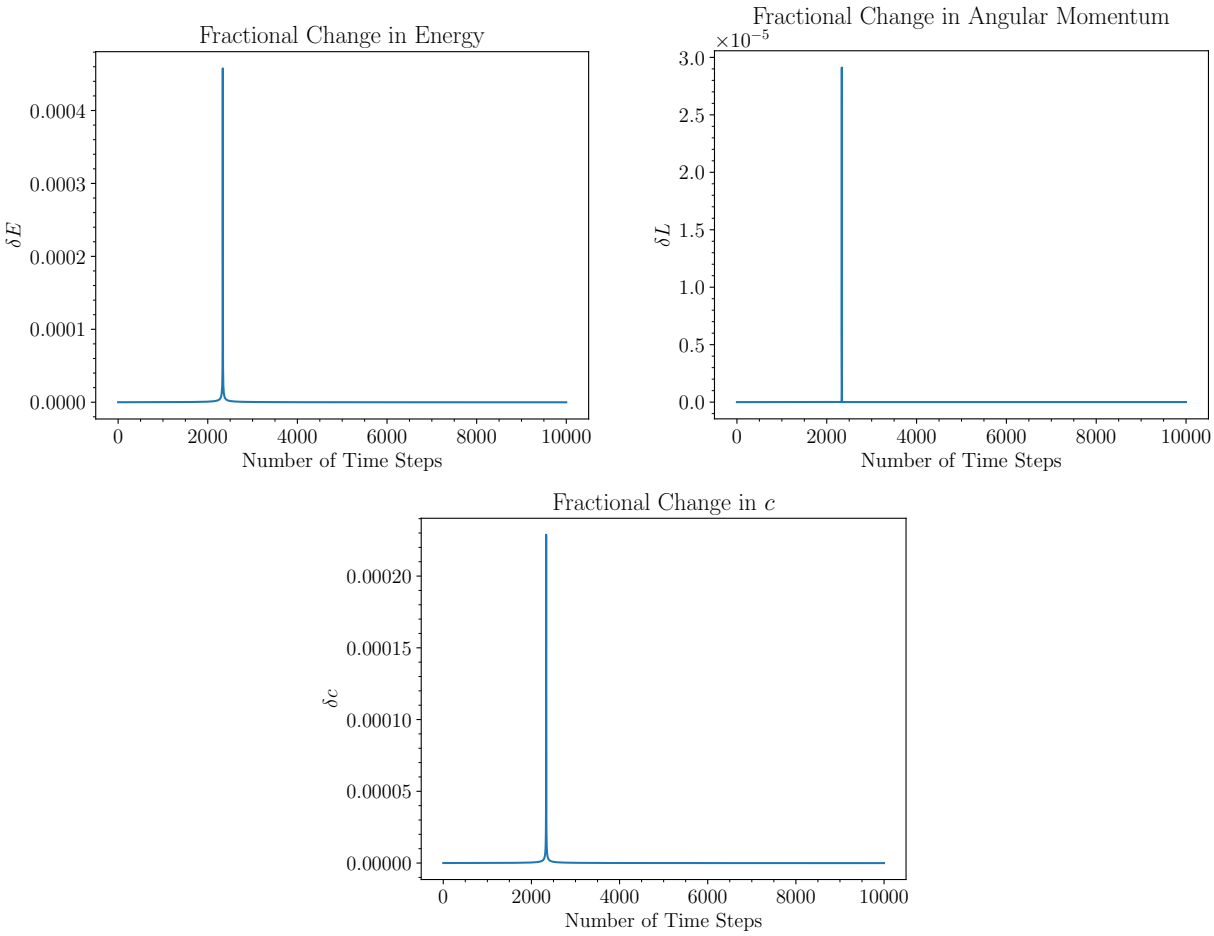

Figure 4: Plots showing the fractional change in energy, angular momentum, and the speed of light c for the configuration in the last plot of Figure 9. We calculated each quantity at each time step of the numerical differential equation solver (a total of 10^7 steps), but plotted 10^4 entries for each.

2.2.5 2D Root Finding with `deflecThor`

Our next step is to find solutions to the Virbhadra-Ellis lens equation for a given lens system and source position to answer questions $\mathbf{Q_{III}}$ and $\mathbf{Q_{IV}}$. We note that finding solutions to the equation is equivalent to finding the roots $\boldsymbol{\theta}$ to the following equation:

$$\tan(\boldsymbol{\theta}) - \frac{d_{LS}}{d_S}\left(\tan(\boldsymbol{\theta}) + \tan(\hat{\boldsymbol{\alpha}} - \boldsymbol{\theta})\right) - \tan(\boldsymbol{\beta}) = 0. \tag{10}$$

In this equation, the source position $\boldsymbol{\beta}$ is known. The deflection angle is a function of a light ray's impact parameter with each mass, and hence is a function of $\boldsymbol{\theta}$. Therefore, to find the roots of this equation, we implemented a 2D root-finding algorithm in conjunction with `pygravlens`[4]. `pygravlens` is a numerical routine that calculates the angular positions of the solutions to the small-angle equation, Eq. (1), with the *General Relativistic* deflection angle, given the source angular position and the lens positions and masses.

For a given lens system and source, we first used `pygravlens` to calculate the total number of images and their positions $\boldsymbol{\theta}_i$ in the small-angle relativistic framework. Although we expect there to be differences between the predicted image positions in the Newtonian and relativistic cases, the $\boldsymbol{\theta}_i$ provide initial guesses for the root-finding algorithm, constraining the region over which it searches for roots of Eq. (10). Therefore, this technique enables us to look for all of the solutions, if multiple exist, to the Virbhadra-Ellis equation.

3 Results

3.1 Analyzing the Newtonian Deflection Angle

Using the Newtonian deflection angle, Eq. (8), we answer $\mathbf{Q_I}$, $\mathbf{Q_{II}}$, and part of $\mathbf{Q_{III}}$. To do so, we need to see if the deflection angle diverges at $b = 0$, and if not, what the maximum value of the deflection angle is.

Since $\tilde{r}, b > 0$, $|\hat{\boldsymbol{\alpha}}(b)| > 0$ for all b. Now, we consider its derivative:

$$\frac{d\,|\hat{\boldsymbol{\alpha}}(b)|}{db} = -\frac{2\tilde{r}}{b^2 + \tilde{r}^2} < 0 \qquad \forall b \geq 0. \tag{11}$$

Since the derivative is strictly negative and $|\hat{\boldsymbol{\alpha}}(b)| > 0$ for all b, it follows that $|\hat{\boldsymbol{\alpha}}(b)|$ is a strictly decreasing function. Moreover,

$$|\hat{\boldsymbol{\alpha}}(0)| = 2\arcsin\left(\frac{\tilde{r}}{\sqrt{\tilde{r}^2 + 0}}\right) = 2\arcsin\left(\frac{\tilde{r}}{\tilde{r}}\right) = 2 \cdot \frac{\pi}{2} = \pi. \tag{12}$$

This shows that unlike the relativistic deflection angle considered by [7, 10, 14], the Newtonian deflection angle is bounded, and certainly does not diverge at the position of each point mass. Figure 5 depicts these results.

Since the proof of the lower bound in [10] is built on the assumption that the time-delay and hence the deflection diverges at each point mass and we showed this not to be the case for our equation, we find that the mathematical analysis and techniques presented in [10], in their original form, do not apply to our problem.

Secondly, infinitely many "relativistic" images are formed when an incoming light ray is deflected by an angle of $2\pi n$, for some positive integer n [3, 16]. These images are possible in the General Relativistic framework since, as Figure 5(a) depicts, the deflection angles can get arbitrarily large.

[4] https://github.com/chuckkeeton/pygravlens/blob/main/pygravlens.py

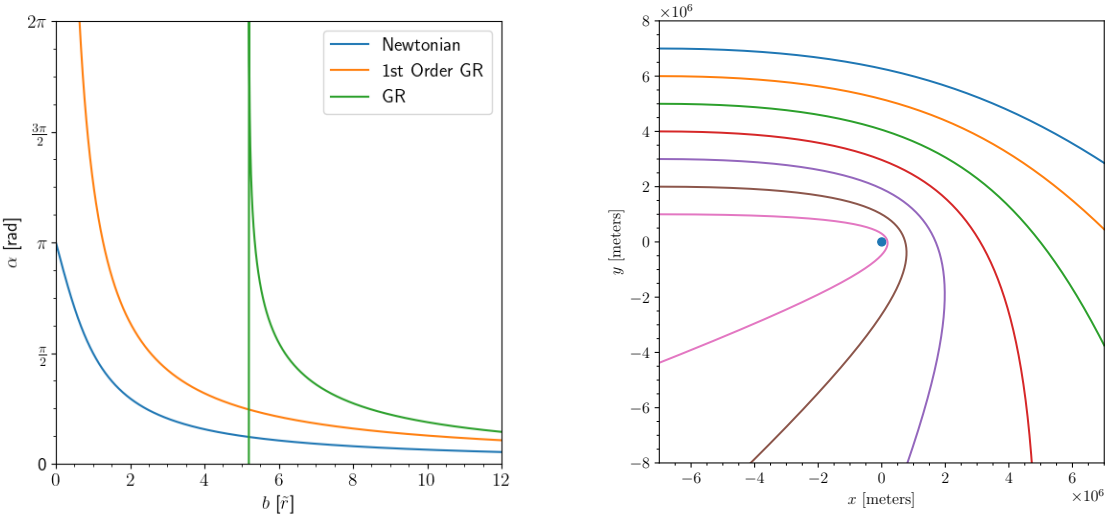

Figure 5: **(a)** Comparison of Eq. (8), the 1st order GR approximation ($4GM/c^2b$), and the full GR deflection angle. The horizontal axis is expressed in terms of $\tilde{r}$. The full GR angle (see [6]) diverges at $b = 3\sqrt{3}r_s$. **(b)** Physical implications of (a). These plots show light ray trajectories for various impact parameters. Each deflection angle is less than π rad.

However, because the Newtonian deflection angle supports a maximum angle of π radians, we find that relativistic images are *not* possible in the Newtonian framework, as expected.

Since the maximum deflection angle is π (in which case, the light ray reverses its direction of travel), it is heuristically possible to construct configurations of g point masses that produce multiple images. Figure (6) shows a rough depiction of this result.

If we presume that multiple images are possible and that the number of images satisfies the lower bound of $g+1$, then the boundedness of $\hat{\boldsymbol{\alpha}}$ means that we would have to modify the techniques and proofs given in [10] since it assumes that the angle diverges.

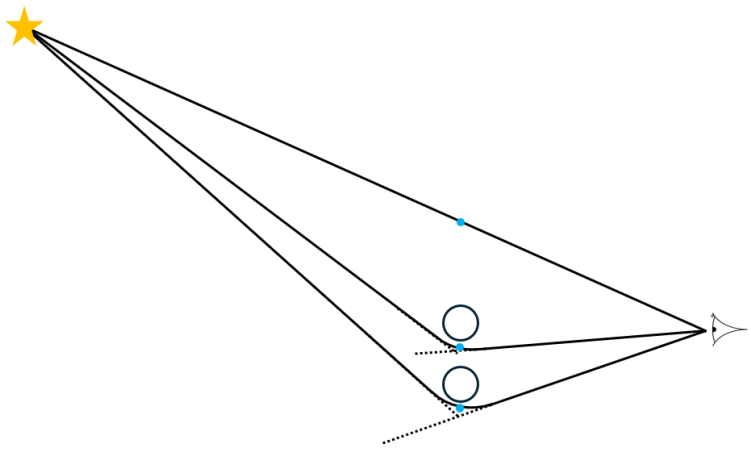

Figure 6: Rough depiction of a configuration that could produce multiple images (blue). All of the deflection angles are less than π and are achievable. This configuration produces three images, which saturates the lower bound for 2 point masses.

3.2 Constructing Multiple Images

As mentioned in Section 3.1, it is possible that our lens equation (5) can produce multiple solutions. Therefore, using the methodology discussed in Section 2.2.5, we constructed various configurations for different numbers, g, of point masses. We assume that each of the point masses have the same mass, $M_j = 1\,M_\odot$. Since the maximum lensing effects occur when the lens is roughly halfway between the source and the observer, we assume $d_{LS} = d_L = (1/2)d_S$ in each of the following examples. For concreteness, we choose $d_{LS} = 10^{11}$ m. We found that for much larger distances, e.g., $d_{LS} \sim 10^{19}$ m (consistent with the typical microlensing distances), our routines need to be made more efficient. We are currently working on making these changes.

3.3 Plots of Various Configurations

Here, we present a few different configurations consisting of $g = 1, 2$, and 3 point masses. Table 1 provides the bounds on the number of images for each g.

	Lower Bound $(g+1)$	Upper Bound $(5g-5)$
$g = 1$	2	—
$g = 2$	3	5
$g = 3$	4	10

Table 1: Table of lower and upper bounds for g point masses, for $g = 1, 2, 3$. There are no upper bounds for $g = 1$; we may produce infinitely many images (e.g., an Einstein Ring).

3.3.1 One Mass $(g = 1)$:

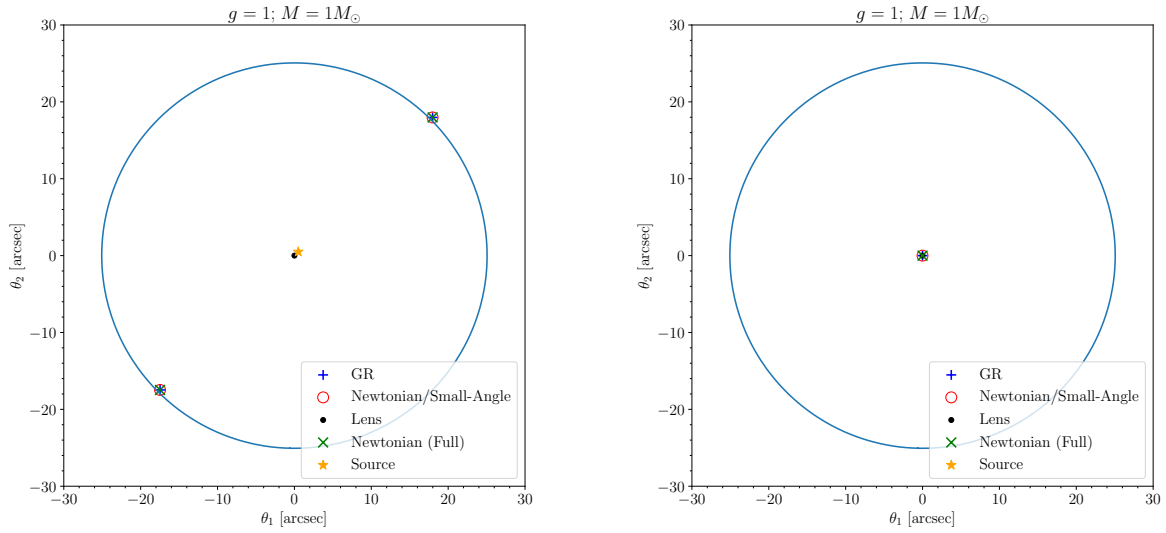

Figure 7: Plots depicting the predicted image positions in different frameworks for one mass. The blue curve depicts the critical curve. Both images saturate the lower bound. **(a)** Two predicted image positions. We do not observe the source. **(b)** One image is close to the lens, and another image of the source is at the source angular position, $\boldsymbol{\beta} = (10^5, 0)''$ (outside the frame).

3.3.2 Two Masses ($g = 2$):

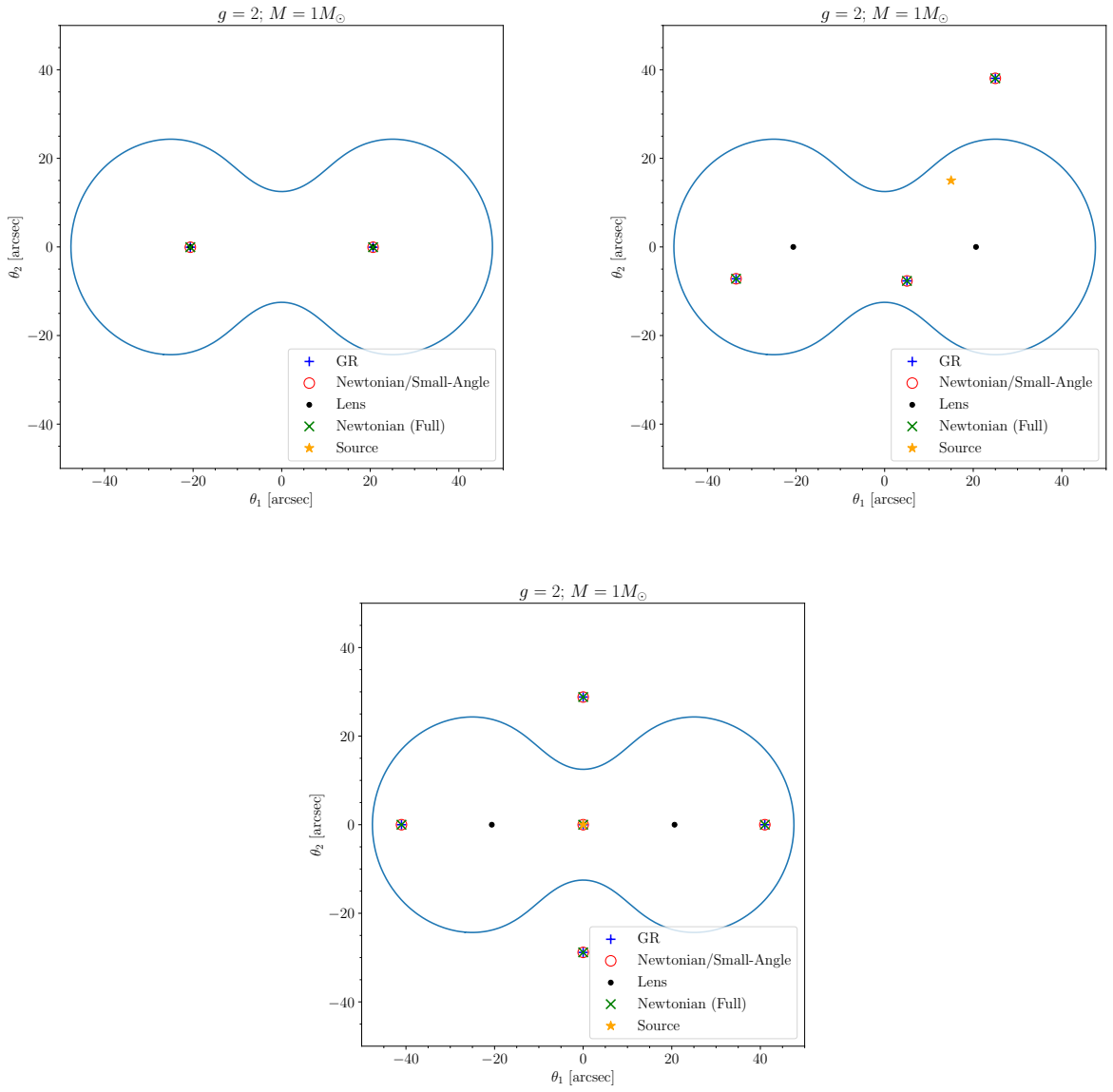

Figure 8: Example configurations for two masses. **(a)** Configuration saturating the lower bound, with the third image outside the top frame of the plot at $\boldsymbol{\theta} = (0, 10^5)''$. **(b)** Another configuration with three images. **(c)** Configuration saturating the upper bound of five images.

3.3.3 Three Masses ($g = 3$):

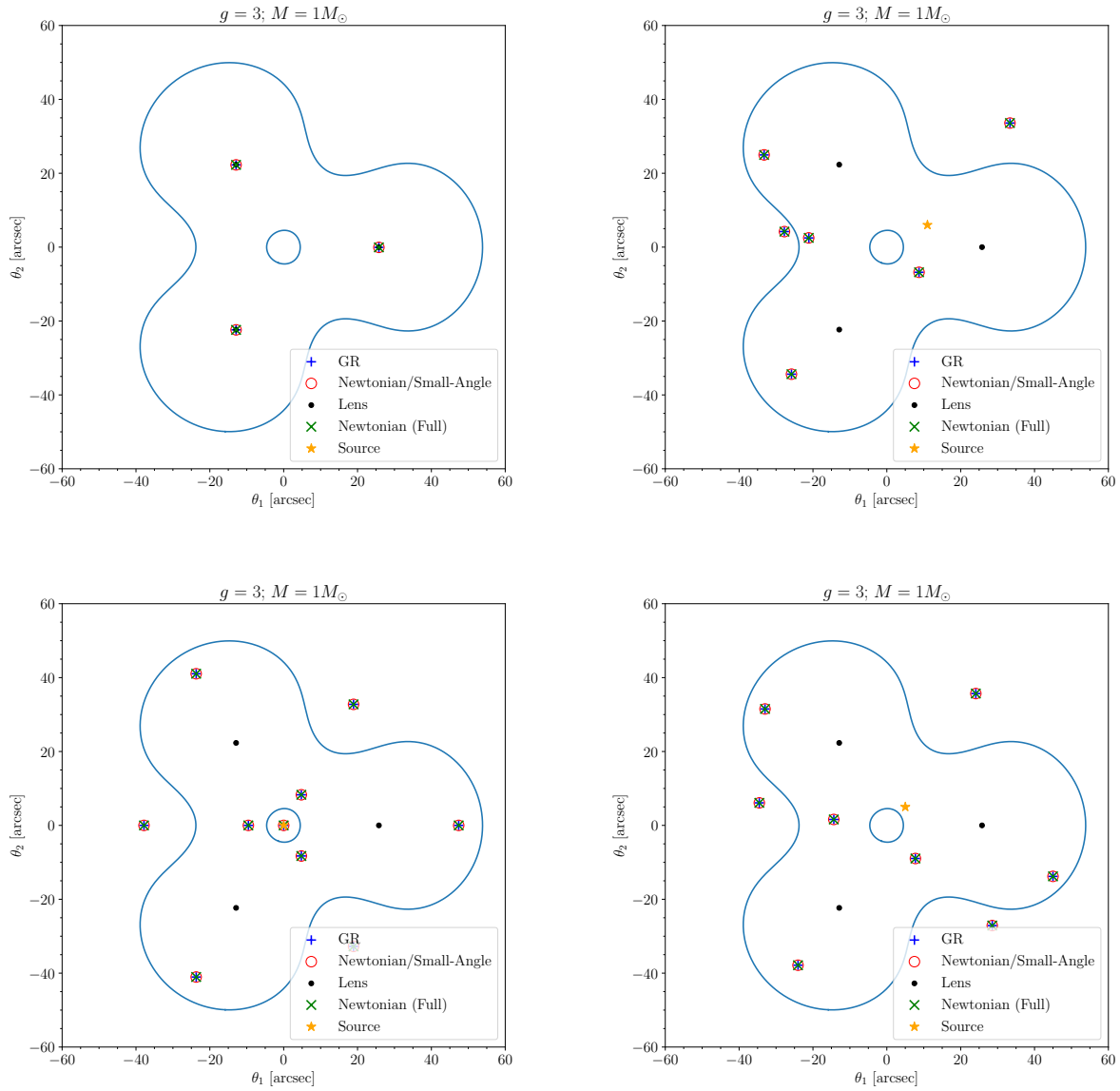

Figure 9: Various configurations with $g = 3$ point masses. From top left, in clockwise direction: **(a)** A configuration that saturates the lower bound, with the fourth image of the source far outside of the frame, to the right; **(b)** A configuration with six images; **(c)** A configuration with eight images; **(d)** A configuration with ten images (one image is behind the legend).

3.4 Discussion of Plots

In short, we showed that the Virbhadra-Ellis equation can have multiple distinct solutions when working in the Newtonian framework. Figures 7, 8, and 9 show some sample configurations of lens systems and the corresponding solutions. We compared the image positions for the Virbhadra-Ellis equation with the corresponding solutions to the small-angle relativistic equation 1 and the small-angle Newtonian equation (same as Eq. 1, except we now use the Newtonian deflection angle). We found that the positions were generally consistent with each other, with an average difference of 10^{-3}" between the Newtonian and GR positions, and $< 10^{-5}$" between the two Newtonian predictions. To investigate if these differences were caused by numerical errors, we examined the precision of the numerical integrators used in `deflecThor` and the root-finding algorithm `scipy.optimize.fsolve()` used to solve our equation. We found that increasing the precisions did not reduce the average difference, which suggests that they are likely reflecting the difference in physics underlying the relativistic and Newtonian frameworks.

Most importantly, our plots show that the number of solutions to the Virbhadra-Ellis equation can saturate the known bounds for the small-angle relativistic equations (Theorems 1 and 2). Therefore, we make the following conjecture:

Conjecture 1 (Number of Solutions to the Virbhadra-Ellis Equation)**.** Let N be the number of solutions to the Virbhadra-Ellis equation, where $\hat{\boldsymbol{\alpha}}$ is the Newtonian deflection angle for a system of g point masses in a single plane. Then N satisfies the same bounds as found by [7, 10, 14]; i.e.,

$$g + 1 \leq N \leq 5g - 5.$$

4 Conclusion

To summarize, we have examined various questions regarding the number of solutions (astrophysically, the number of lensed images) to the Virbhadra-Ellis lens equation, Eq. (5) in the Newtonian framework. In doing so, we have provided a framework for a subsequent mathematical analysis of this problem.

Our most important finding is that our equation can have multiple solutions, similar to the small-angle relativistic equation studied before by [7, 10, 14]. We exhibited configurations consisting of $g = 1, 2$, and 3 point masses in a single plane that saturated the known bounds for the small-angle relativistic configurations in Section 3.3. We also found that the positions predicted by the different equations were generally consistent with each other, with a small difference of 10^{-3}", which we showed was likely not to be numerical. Our results led us to conjecture that our equation satisfies the known bounds for the small-angle relativistic case.

After deriving the Newtonian deflection angle for a single mass in Section 3.1, we showed that it is finite for all impact parameters b, with a maximum of π radians. First, this implies that while our equation can produce multiple images, it cannot produce *infinitely* many, unlike in the GR case. Second, the boundedness of the deflection angle in the Newtonian case implies that the associated time-delay surface does not diverge near each point mass, contradicting one of the key assumptions made in the analysis of the lower bound by [10].

From a mathematical standpoint, these are exciting results; although the equations we examined look and "behave" differently from the small-angle relativistic equation, Eq. (1), we believe that it satisfies the same bounds on the number of solutions that applies for Eq. (1). This merits a serious mathematical analysis, which could help us verify or derive these bounds rigorously. While

the specific details of such an analysis are not clear now, our numerical analysis shows that it must be substantially different from existing analyses. Therefore, our work can serve to motivate, guide, and inspire these new mathematical developments.

In the future, we would like to explore these new developments via collaborative efforts with mathematicians working in adjacent fields, using our current work as a foundation. With the results we will obtain through such work, we will explore other, mathematically and astrophysically, interesting variations of this problem. For instance, we can consider a general system of g masses on *different* lens planes as studied in [5]. We can also examine the Virbhadra-Ellis equation in the complete relativistic case and seek explicit counting formulas for the number of images. These work could inspire new applications to the theory of microlensing and strong-lensing, and drive astrophysical research. More broadly, through this project and any subsequent work it inspires, we can continue to explore the rich interactions between mathematics and astrophysics.

5 Acknowledgements

I would like to thank my advisor, Professor Charles Keeton, for his support and guidance over the past three years. What started as a summer research project through the Aresty Summer Science Program has blossomed into one of my most treasured experiences. I would also like to thank the members of the Rutgers Lensing Group: Dr. Somayeh Khakpash, Lana Eid, and Satyajit Gade for their helpful perspectives, feedback, and support. I also acknowledge the Department of Physics and Astronomy, particularly Professor Jolie Cizewski, for their support of undergraduate research and for making this opportunity possible. Last, but certainly not the least, I would like to thank my family: my parents for their enduring patience, support, and belief throughout this journey, and my twin sister for always standing by my side and helping me review this thesis despite her own workload and deadlines.

References

[1] Aazami, A. B., & Natarajan, P. 2006, Monthly Notices of the Royal Astronomical Society, 372, 1692–1698, doi: 10.1111/j.1365-2966.2006.10991.x

[2] Blandford, R., & Narayan, R. 1986, The Astrophysical Journal, 310, 568, doi: 10.1086/164709

[3] Bozza, V. 2010, General Relativity and Gravitation, 42, 2269, doi: 10.1007/s10714-010-0988-2

[4] Frye, B. L., Pascale, M., Foo, N., et al. 2023, The Astrophysical Journal, 952, 81, doi: 10.3847/1538-4357/acd929

[5] Keeton, C. R., Lundberg, E., & Perry, S. 2023, Journal of Mathematical Physics, 64, 032502, doi: 10.1063/5.0124892

[6] Keeton, C. R., & Petters, A. O. 2005, Physical Review D, 72, 104006, doi: 10.1103/PhysRevD.72.104006

[7] Khavinson, D., & Neumann, G. 2006, Proceedings of the American Mathematical Society, 134, 1077. http://www.jstor.org/stable/4098072

[8] Madhava, A., & Keeton, C. R. 2024, The Astrophysical Journal, 975, 287, doi: 10.3847/1538-4357/ad7eb6

[9] Mróz, P., Poleski, R., Gould, A., et al. 2020, The Astrophysical Journal, 903, L11, doi: 10.3847/2041-8213/abbfad

[10] Petters, A. O. 1992, Journal of Mathematical Physics, 33, 1915, doi: 10.1063/1.529667

[11] Petters, A. O., & Werner, M. C. 2010, General Relativity and Gravitation, 42, 2011, doi: 10.1007/s10714-010-0968-6

[12] Raney, C. A., Keeton, C. R., & Brennan, S. 2020, Monthly Notices of the Royal Astronomical Society, 492, 503, doi: 10.1093/mnras/stz3116

[13] Raney, C. A., Keeton, C. R., & Zimmerman, D. T. 2021, Monthly Notices of the Royal Astronomical Society, 508, 5587, doi: 10.1093/mnras/stab2857

[14] Rhie, S. H. 2003, arXiv e-prints, astro, doi: 10.48550/arXiv.astro-ph/0305166

[15] Schneider, P. 1985, Astronomy and Astrophysics, 143, 413

[16] Virbhadra, K. S., & Ellis, G. F. R. 2000, Phys. Rev. D, 62, 084003, doi: 10.1103/PhysRevD.62.084003

[17] Zimmerman, D. T., Keeton, C. R., & Raney, C. A. 2021, Monthly Notices of the Royal Astronomical Society, 508, 5602, doi: 10.1093/mnras/stab2858

A Deriving the Newtonian Deflection Angle

In this section, we provide a formal derivation of the Newtonian deflection angle Eq. (8). We consider a point mass M situated at the origin, and an incoming photon whose trajectory has an impact parameter b with M. The energy $\tilde{E}$ and angular momentum $\tilde{L}$ per unit mass of the photon are,

$$\tilde{E} = \frac{1}{2}v^2 - \frac{GM}{r} = \frac{1}{2}\dot{r}^2 + \frac{1}{2}r^2\dot{\theta}^2 - \frac{GM}{r}. \tag{13}$$

$$\tilde{L} = r^2\dot{\theta}. \tag{14}$$

Substituting the angular momentum into the expression for energy and solving for $\dot{r}$, we obtain:

$$\dot{r} = \pm\left(2\tilde{E} - \frac{\tilde{L}^2}{r^2} + \frac{2GM}{r}\right)^{1/2}. \tag{15}$$

First, we find the closest distance, r_0 between the mass and the photon by setting $\dot{r} = 0$:

$$\dot{r} = 0 \implies r = -\frac{GM}{2\tilde{E}} + \sqrt{\frac{\tilde{L}^2}{2\tilde{E}} + \frac{G^2M^2}{4\tilde{E}^2}}. \tag{16}$$

Using the expression for the angular momentum, we find

$$\frac{d\theta}{dr} = \pm\frac{\tilde{L}}{r^2}\left(2\tilde{E} - \frac{\tilde{L}^2}{r^2} + \frac{2GM}{r}\right)^{-1/2}.$$

The initial energy of the photon was $(1/2)c^2$, while its angular momentum as it passed the impact parameter distance was bc. Assuming energy and angular momentum conservation, the above expression simplifies to,

$$\frac{d\theta}{dr} = \pm\frac{bc}{r^2}\left(c^2 - \frac{b^2c^2}{r^2} + \frac{2GM}{r}\right)^{-1/2} = \frac{b}{r^2}\left(1 - b^2r^{-2} + 2\tilde{r}r^{-1}\right)^{-1/2}, \tag{17}$$

where $\tilde{r} = (1/2)r_s = GM/c^2$ and r_s is the "Schwarzschild" radius. Likewise, the closest distance r_0 simplifies to the following expression:

$$r_0 = -\tilde{r} + \sqrt{b^2 + \tilde{r}^2}. \tag{18}$$

Therefore, the Newtonian deflection angle is [6],

$$\begin{aligned} |\hat{\boldsymbol{\alpha}}| &= 2\int_{r_0}^{\infty}\left|\frac{d\theta}{dr}\right| dr - \pi \\ &= 2\int_{r_0}^{\infty}\frac{bdr}{r^2(1 - b^2r^{-2} + 2\tilde{r}r^{-1})^{1/2}}dr - \pi. \end{aligned} \tag{19}$$

To simplify this integral, we first make the change of coordinates to $u = r^{-1}$. The new lower limit of integration is 0, while the new upper limit of integration is,

$$r_0^{-1} = \frac{\tilde{r} + \sqrt{\tilde{r}^2 + b^2}}{b^2}. \tag{20}$$

Hence, the deflection angle now becomes

$$|\hat{\boldsymbol{\alpha}}| = 2\int_0^{\frac{\tilde{r}+\sqrt{\tilde{r}^2+b^2}}{b^2}}\frac{bdu}{(1 - b^2u^2 + 2\tilde{r}u)^{1/2}} - \pi. \tag{21}$$

Now, we define the trigonometric substitution,

$$bu = \frac{\sqrt{\tilde{r}^2 + b^2}}{b}\sin(t) + \frac{\tilde{r}}{b} \implies bdu = \frac{\sqrt{\tilde{r}^2 + b^2}}{b}\cos(t)dt.$$

The new integrand is,

$$\begin{aligned} \left(1 - b^2u^2 + 2\tilde{r}u\right)^{-1/2} &= \left(\frac{b^2 + \tilde{r}^2}{b^2}\cos^2(t)\right)^{-1/2} \\ &= \frac{b}{\sqrt{b^2 + \tilde{r}^2}}\cdot\frac{1}{\cos(t)}. \end{aligned} \tag{22}$$

Therefore, the deflection angle becomes, using this substitution,

$$\begin{aligned} |\hat{\boldsymbol{\alpha}}| &= 2\int_{-\arcsin\left(\frac{\tilde{r}}{\sqrt{\tilde{r}^2+b^2}}\right)}^{\pi/2} dt - \pi \\ &= 2\left[\frac{\pi}{2} + \arcsin\left(\frac{\tilde{r}}{\sqrt{\tilde{r}^2 + b^2}}\right)\right] - \pi \\ &= 2\arcsin\left(\frac{\tilde{r}}{\sqrt{\tilde{r}^2 + b^2}}\right). \end{aligned} \tag{23}$$

This is the expression stated in Eq. (8).